Contents lists available at ScienceDirect

Journal of Pipeline Science and Engineering

Inhibition and co-condensation behaviour of 2-mercaptoethanol in top-of-line CO_2 corrosion environments

Mariana C. Folena [a,*], Joshua Owen [b], Iain W. Manfield [c], Hanan Farhat [a], J.A.C. Ponciano [d], Richard Barker [b]

[a] The Corrosion Center of Qatar Environment & Energy Research Institute (QEERI), Hamad Bin Khalifa University Doha 34110, Qatar
[b] Institute of Functional Surfaces (iFS), School of Mechanical Engineering, University of Leeds, Leeds, LS2 9JT, UK
[c] Institute of Molecular and Cellular Biology, Faculty of Biological Sciences, University of Leeds, LS2 9JT, UK
[d] Corrosion Laboratory (LabCorr), Material and Metallurgical Engineering Program, COPPE, Federal University of Rio de Janeiro, Technology Center, Rio de Janeiro, RJ, Brazil

ARTICLE INFO

ABSTRACT

Top of line corrosion (TLC) is a significant problem in oil and gas transportation pipelines, leading to both economic and production loss. Conventional organic corrosion inhibitors typically fail to provide effective protection for this particular type of corrosion. As such, the chemical inhibition of TLC relies on volatile compounds which can partition from the aqueous to the condensate formed at the top of the pipeline. Studies have shown that thiol compounds, through their high affinity for metallic surfaces, are providing effective inhibition in such environments, yet their inhibition mechanism and co-condensation characteristics are yet to be fully determined. This work studies the efficiency, adsorption mechanism and condensation behaviour of 2-mercaptoethanol (2-ME) as a volatile corrosion inhibitor in CO_2-containing TLC environments through a novel direct assessment of condensate chemistry and real-time TLC measurements. Experimental analysis of condensate partitioning is performed through the implementation of a biochemical technique which targets sulphydryl groups, coupled with a miniature electrode configuration for real time, in-situ electrochemical TLC measurements. The proposed assay results in a rapid, cost-effective screening technique that can monitor thiol-based chemistries that condense in conjunction with the water phase. The new developed biochemical methodology identified that from 20 ppm of 2-ME added to the bulk solution, only around 12 ppm was present within the condensate. Additionally, 2-ME addition into the system resulted in a corrosion inhibitor efficiency of 93.8% where the chemical act as a mixed-type corrosion inhibitor. The corrosion and condensation experiments are complemented with surface characterization via XPS and STEM-EDX techniques. The surface characterization analysis showed a compact inner layer containing sulphur which is related to adsorption of the thiol.

1. Introduction

Top of line corrosion (TLC) is a degradation mechanism predominantly encountered in the oil and gas industry. Initiation of TLC requires a stratified flow regime with wet gas transportation and the existence of significant temperature gradient between the hot fluid inside the pipeline and the colder external environment, specifically at points of lower thermal insulation. This temperature difference results in water vapour in the gas phase condensing onto the cooler, upper internal section of the

pipeline. The condensed water can be particularly aggressive as it lacks dissolved salts, some of which are able to buffer the electrolyte, increasing its pH and suppressing corrosivity of the bulk fluid. The absence of such salts typically results in a very low pH condensate (pH < 4), containing dissolved gases such as carbon dioxide (CO_2), hydrogen sulphide (H_2S) and acetic acid (HAc), which attacks the metal wall and can cause severe degradation, particularly in the form of localised corrosion (Folena et al., 2020).

Despite the existence of TLC for decades and its prevalence within

---

the oil and gas industry, the underlying mechanism still remains unclear and there are significant challenges associated with its control. In hydrocarbon transportation via pipelines, the most common method of internal corrosion control is through the deployment of corrosion inhibitors (or surfactants). The chemical structure of these inhibitory molecules is such that they possess an affinity for adsorption at interfaces such as the metal-electrolyte interface. This adsorption process creates a barrier that can inhibit corrosion, with the extent of adsorption (or efficiency) dictated by the properties of the surfactant and its level of interaction with the metal surface and the surrounding environment. In the context of TLC, many of the organic chemistries that successfully control corrosion of steel in bulk fluids typical of oilfield environments fail to successfully suppress corrosion at the metal-condensate interface. This is attributed to the low volatility of the chemistries used, which means that once they are injected into the bulk oil and/or water phase, they remain at the bottom of the line and cannot be effectively transported to the top of the line. For this reason, TLC is one of the most challenging corrosion processes facing the industry. Consequently, there is a clear need to develop an understanding of the underlying mechanism so that the problem can be understood and the conditions conductive to severe TLC can be identified and/or avoided. Furthermore, there also needs to be a concerted effort towards identifying and understanding the behaviour, performance and mechanisms of more volatile inhibitors in controlling TLC.

The corrosion inhibitor chemistries selected to suppress degradation in TLC conditions must have an appreciable vapour pressure to enable them to partition into the condensate within the upper pipeline section. Furthermore, these chemicals must also have the required chemical and/or physical affinity for the steel, as well as a low potential for reaction with organic acids. One branch of chemistries which have recently attracted interest in suppressing TLC and have been proved to be largely successful in laboratory experiments are alkanethiols (Belarbi et al., 2017, 2018). From the open literature, the first study of thiol chemistries as potential vapour corrosion inhibitors (VCIs) in oil and gas environments was performed by Belarbi et al. (2017) whereby two different alkane thiols and a carboxyl-containing thiol (hexanethiol, decanethiol and 11-mercaptoundecanoic acid, respectively) were evaluated for CO_2 TLC corrosion inhibition of carbon steel. TLC tests were performed at a gas temperature (T_{gas}) of 65 °C, a steel surface temperature ($T_{surface}$) of 32 °C and water condensation rate (WCR) of 0.6 mL/(m^2 s) with addition of 100 ppm$_v$ of each compound to the bulk solution 6 min prior to adding the mass loss carbon steel samples. The research group identified that the longest chain molecules proved to be more effective reducing the general corrosion rate (CR) from 1 mm/a to less than 0.03 mm/a after 2 d of exposure. The inhibitor persistence was evaluated through dilution by renewing the solution at a flow rate of 1.7 L/min with the uninhibited solution after 2 d of tests and carrying the test for another 2 d. Both the long chain thiols and 11-mercaptoundecanoic acid showed strong persistency, with corrosion rates of 0.02 and 0.04 mm/a, respectively, even after the solution dilution over 2 d. The inhibitor persistency was attributable to the high hydrophobicity which provides inhibitor/steel affinity stronger than inhibitor/water resulting in an excellent barrier against corrosive species from attacking the underlying carbon steel substrate. Despite a lack of quantification as to the extent of co-condensation of the inhibitor, or an analysis of whether localised corrosion was suppressed in such environments, this was perhaps study indicated the high potential for thiol chemistries to provide effective inhibition under CO_2 TLC conditions.

In a subsequent study by Belarbi et al. (2018), the influence of different TLC operating parameters (e.g., different WCRs, presence of monoethylene glycol (MEG), H_2S, and hydrocarbons) on decanethiol inhibition efficiency were evaluated. Decanethiol was shown to be an efficient VCI against TLC independently of the WCR and even in the presence of MEG and traces of H_2S. However, when evaluating decanethiol in the presence of non-polar solvents, (1 wt% CO_2-saturated NaCl (1.2 L) with n-heptane (0.6 L)) at a WCR of 0.2 mL/m^2 s. The final corrosion rates observed after 4 d of exposure were 0.14 mm/a and 0.13 mm/a respectively for uninhibited and inhibited system. These values were twice as high when compared to tests performed at same conditions without heptane (CR = 0.07 mm/a). This inferior inhibition efficiency was believed to be at least partly attributed to partial diffusion of the thiols into the oil phase (heptane) since the lipophilic thiol tail has higher affinity to oil than water (Belarbi et al., 2018).

Although thiols have been vastly studied as a corrosion inhibitor for copper in acid solutions, substantially less information exists in the open literature regarding its efficiency in inhibiting the corrosion of iron and steel, particularly in CO_2-containing environments, despite its presence as a sulphur synergist in many fully formulated oilfield inhibitor chemistries (Behpour and Mohammadi, 2012; Feng et al., 1997; Quan et al., 2002).

Notwithstanding, recent studies have been conducted evaluating the corrosion inhibition of mild steel in acid medias by aromatic thiols. Bentis et al. (2005) evaluated the corrosion inhibition of mild steel in 1 M hydrochloric acid solution by 2,5-bis(n-thienyl)-1,3,4-thiadiazoles(n-TTH) while Musa et al. (2010) studied the corrosion inhibition of mild steel in a 2.5 mol H_2SO_4 solution by 4-amino-5-phenyl-4H-1,2,4-trizole-3-thiol (APTT), both at temperatures ranging from 30 °C to 60 °C. The authors concluded that the aromatic thiol showed excellent inhibition performance as a mixed-type inhibitor in acid media. Inhibitor efficiencies of up to 89.9% and 97.2%, respectively for APTT and n-TTH at the highest tested temperature were found due to addition of an appropriate concentration of thiols. Both studies also concluded that the inhibition efficiencies increased with inhibitor concentration whilst proportionally reducing with temperature.

Concerning oil and gas applications, a recent study on mercaptoalcohols has shown improved corrosion inhibition properties of both general and localised corrosion when tested in oil and gas pipelines, especially in high shear and flow systems (Young Soo Ahn, 2003). A sparged beaker test using complex brine and Isopar® (paraffinic hydrocarbon) in a 80/20 ratio and 10 ppm 2-mercaptoethanol (2-ME) and 2-MP was conducted at 71 °C and 1 atm CO_2 saturation for 20 h. Results showed a corrosion inhibition efficiency of 87.2% for 2-mercaptoethanol and 86% inhibition efficiency when using 2-mercaptopropanol. According to the patent experiments, mercaptoalcohols, specifically 2-ME and 2-MP protect the corrosion of iron and steel by establishing a persistent film on the metallic surface though dissulfide formation (Young Soo Ahn, 2003).

An advantage of using low-molecular weight mercaptoalcohols, such as 2-ME, is that they have high solubility in water, ethanol, and hydrocarbons, thus serving as a corrosion inhibitor across a range of fluids. Furthermore, 2-ME also has a high volatility, which raises the possibility of using it as a potential VCI.

The main protection feature of thiols discussed in the literature is its ability to adsorb (via interaction with the polar S-heteroatom on the thiol head and the metal surface), creating a self-assemble monolayer (SAM) even at room temperature (Vericat et al., 2014). This monolayer generates a highly protective film against corrosion that has been reported to be either chemically or physically adsorbed on the metal surface depending upon the metal-electrolyte interfacial environment. Many studies indicate that the adsorption behaviour of thiol on non-iron metal samples follows Langmuir adsorption isotherm (chemisorption mode), however with regards to thiol adsorption on iron and carbon steel surfaces, physisorption, chemisorption and even mixed chemical-physical adsorption mechanisms have all been proposed. Table 1 presents a summary of the adsorption modes reported for thiol compounds on metallic surfaces.

Potentially one of the main reasons of such differing observations relating to thiol adsorption mode on iron and carbon steel is due to the difficulty in conclusively identifying the presence or absence Fe-SR' chemical bond by conventional surface analysis techniques. Hence, many studies have relied on the calculation of the free energy adsorption (ΔG^o_{ads}) for such purposes.

Table 1
Summary of the adsorption modes of different thiols on different metal substrates.

Author	Compound	Metal substrate	Adsorption mode
Ehteshamzadeh and Shahrabi (2006)	1-Decanethiol	Carbon steel	Physical
Belarbi et al. (2017)	1-Decanethiol	Carbon steel	Physical
Barker (2012)	2-Mercaptoethanol	Carbon steel	Chemical
Kudelski (2003)	2-Mercaptoethanol	Au, Ag, Cu	Chemical
Bentis et al. (2005)	2-TTH and 3-TTH	Carbon steel	Chemical
Uehara and Aramaki (1991)	Benzenethiol and phenylmethanethiol	Iron	Chemical
Volmer-Uebing and Stratmann (1992)	1-Decanethiol and propanethiol	Iron	Chemical
Döner et al. (2011)	2-amino-5-mercapto-1,3,4-thiadiazole and 2-mercaptothiazoline	Carbon steel	Chemical (predominantly) and physical

Since this chemical bond is said to be a result of the cleavage of the thiol S-H due to the interaction of the compound with the metallic surface, most authors state that the molecule undergoes chemical adsorption based on a lack of observation of the free thiol binding energy from surface sensitive techniques such as Raman and X-ray photoelectron spectroscopy (XPS) (Bentis et al., 2005; Uehara and Aramaki, 1991; Volmer-Uebing and Stratmann, 1992). However, other authors have stated that the absence of an Fe-S bond suggests an electrostatic interaction with the positively charged metal surface and the negatively charged thiol head (Belarbi et al., 2017). This analysis was conducted in TLC conditions for steel samples which were exposed to the vapour phased produced from a 1 wt% NaCl CO_2-saturated containing 400 ppm_v of decanethiol, with the analysis being performed by XPS. The authors suggested physisorption of decanethiol on the metal surface since there was no binding energy peak belonging to Fe-S in both Fe 2p and S 2p XPS spectra (Belarbi et al., 2017).

In contrast to this observation, Fe-S bonds were observed by XPS analysis when studying the adsorption of decanethiol and propanethiol on iron in a surface analytical and electrochemical study by Volmer-Uebing and Stratmann (1992). The authors concluded that both thiols can be chemisorbed onto oxide-free iron surfaces as observed in both XPS and Auger depth analysis. However, if oxide layers are present on the iron surface prior to thiol adsorption, only high quantities of sulfonate ions were detected. These sulfonates were suggested to be a result of the oxidation of free mercaptan (-SH) that did not interact with the pre-oxidized iron surfaces. These differing observations depending upon the initial or evolved conditions of the steel surfaces may explain the differing observations within literature for the adsorption of thiols onto iron and steel in acidic media.

It is clear that various thiols have been studied recently as VCIs to mitigate TLC in oil and gas fields. However, although these chemicals show promise due to their volatility and adsorption characteristics, their mechanisms of inhibition are yet to be fully understood. For example, to date, no research has been conducted to quantify the amount of thiol which partitions into the condensate to protect the steel from corrosion, nor has the effect of thiols on localised corrosion in TLC environments been considered. Measuring this concentration will help to understand the transport mechanism of thiol chemistries to the top of the line and consequently help to better select and optimise bulk fluid dose rates to ensure adequate top-of-line corrosion inhibition.

This study focuses on understanding the general and localised corrosion inhibition mechanism of 2-ME for carbon steel in TLC environments. A rapid screening technique using a bio-chemical 5,5′-dithiobis-(2-nitrobenzoic acid) (DTNB) assay is optimised and utilised to measure the concentration of 2-ME within the condensate, enabling determination of the extent to which this chemical is able to reach and partition into the fluid at the top of the line, providing new insight into the inhibition process. Align with that, surface characterization is performed in order to better evaluate the inhibitor adsorption on the steel surface as well as its efficiency regarding inhibition of pit initiation/propagation.

2. Experimental setup

Electrochemical and mass loss experiments were performed in the present work to evaluate the corrosion inhibition efficiency of 2-ME in TLC environments, to understand both the mechanism of protection and to evaluate the capability of the rapid colorimetric technique in understanding the extent of inhibitor co-condensation within the condensate. All tests (electrochemical, gravimetric, and colorimetric) were performed at least in triplicate to ensure the experimental results are statistically reliable.

2.1. Top of line corrosion rig and method

A laboratory scale TLC rig previously developed (De Carvalho et al., 2019) was used in this study, with the schematic drawing provided in Fig. 1. The setup consists of a 2 L glass cell with a specific custom lid integrated with an internal channelled matrix, allowing flow of refrigerant to cool the surface of the TLC specimens to specific temperatures. Test specimen slots machined into the channelled lid enable three steel specimens to be inserted into the system, simulating the 12 oclock position of a horizontal 6-inch (152.4 mm) diameter pipeline (Folena et al., 2020; De Carvalho et al., 2021). Both mass loss and electrochemical measurements are possible in the system, with both techniques being utilised in this study. The preparation of test specimens and the configuration of the miniature electrodes used for real time corrosion measurements in the TLC system are discussed in the following sections.

A full description of rig assembly, and its validation as a new TLC test method can be found in previous published papers (Folena et al., 2020; De Carvalho et al., 2021).

The condensate collector is continuously deaerated with CO_2 gas throughout the test to avoid any undesired reaction which could affect the chemical analysis of the condensate (i.e., the reaction of the thiol compound with oxygen).
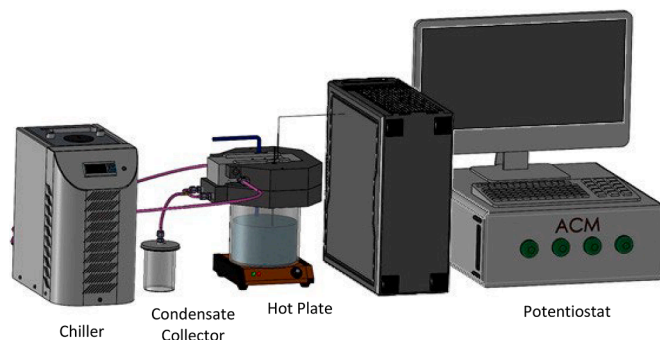

Fig. 1. Schematic of the entire TLC experimental setup adapted from Folena et al. (2020).

2.2. Test specimen materials, preparation and configuration of the miniature electrodes

Mass loss coupons and electrochemical test specimens (shown in Fig. 2) were used in order to obtain both integrated and real-time corrosion rate data, respectively. The mass loss specimens consisted of cylindrical coupons 10 mm in diameter and 6 mm in thickness, with an exposed area to the vapour phase of 0.00785 cm^2. All test specimens were manufactured from the same API 5L X65 carbon steel stock bar, which possessed a ferritic-pearlitic microstructure, with the chemical composition shown in Table 2.

The electrochemical tests were performed by using previously developed solid state miniature electrodes (Folena et al., 2020; De Carvalho et al., 2021) which allows electrochemical tests to be performed in condensation systems. The working electrode consisted of cylindrical pin, 1 mm in diameter and 6 mm in thickness, with an exposed area to the vapour phase of 0.00785 cm^2, whilst the reference electrode and auxiliary electrode consisted of 1 mm thick Hastelloy® c-276 wires, individually isolated and assembled as shown in Fig. 2. A full description of the miniature three-electrode setup, used to monitor the changes in corrosion rate throughout the course of the present experiments, can be found in two previous paper (Folena et al., 2020; De Carvalho et al., 2021).

2.3. Electrochemical measurements

Electrochemical measurements were performed using a miniature three-electrode setup in conjunction with a ACM Gill 8 potentiostat. Three electrochemical techniques were implemented in total. Linear polarisation resistance (LPR) and electrochemical impedance spectroscopy (EIS) were employed to determine the in-situ corrosion rate of the X65 carbon steel specimens. LPR measurements were performed by polarizing the sample ±15 mV vs. the open circuit potential (OCP) at a scan rate of 0.25 mV/s to obtain a polarisation resistance (R_p) and were undertaken every 20 min. The solution resistance (R_s) was measured over the course of the experiment using EIS. These measurements were performed using an amplitude of ±15 mV vs. the OCP and the frequency range from 20 kHz to 0.1 Hz. These parameters were chosen considering previous work which have shown that the system is stable enough to perform such analysis (Folena et al., 2020; De Carvalho et al., 2019). The value of R_p was corrected by subtracting the R_s value, to obtain the
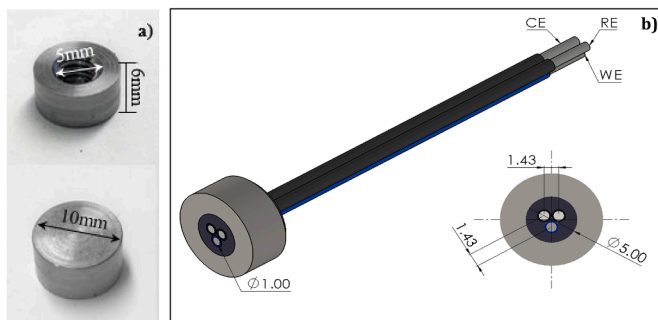

Fig. 2. (a) Mass loss specimens and (b) developed miniature electrodes consisting of two Hastelloy® c-276 wires as reference and counter electrodes and a X65 steel wire, isolated and flush mounted inside a larger X65 specimen (adapted from Folena et al. (2020)).

charge transfer resistance (R_{ct}) which is then used in the Stern-Garry in conjunction with Faraday's Law to determine the corrosion rate with time.

After completion of each 20 h experiment, Tafel polarization curves were collected by performing individual anodic and cathodic sweeps (on separate test specimens), starting from OCP and scanning to −150 mV vs. OCP, for the cathodic branch, and to +150 mV vs. OCP, for the anodic branch, at a scan rate of 0.5 mV/s. From the polarization curves produced, it was possible to determine the anodic (β_a) and cathodic (β_c) Tafel constants in mV/dec by measuring their respective gradient over regions where linearity was observed (on an E vs. log(i) plot). The Stern-Geary coefficient (B), for each experiment was determined, followed by the corrosion current density (i_{corr}) (Eq. (1)):

$$i_{corr} = \frac{B}{R_{ct}} = \frac{1}{R_{ct}} \frac{\beta_a|\beta_c|}{2.303(\beta_a + |\beta_c|)} \qquad (1)$$

Where β_a is the magnitude of the anodic Tafel constant, and β_c is the magnitude of the cathodic Tafel constant (determined from separate experiments). The value of i_{corr} was then used in conjunction with Faraday's Law and an appropriate conversion factor to obtain the corrosion rate in mm/a, as shown in the Eq. (2), which was converted into a rate of thickness loss in mm/a, in accordance to ASTM G102 (ASTM, 2004).

$$CR = K \frac{i_{corr} M_{Fe}}{nF\rho} \qquad (2)$$

Where K is a conversion factor to obtain corrosion rate (mm/a) ($K = 3.16 \times 10^8$); M_{Fe} is the molar mass of iron (55.8 g); n is the number of electrons freed in the corrosion reaction (2 electrons – Fe^{2+}) and ρ is the density of steel (7.87 g/cm^3).

From analysis of the CR vs. time curves produced from the electrochemical measurements, an average corrosion rate (ACR) was determined over the duration of each 20 h experiment, making it possible to compare the results obtained with the mass loss experiments performed in this study, as well as the work of other researchers.

2.4. Test conditions

Based on previous TLC electrochemical tests a gas temperature (T_{gas}) of 70 °C and external temperature (T_{est}) of −10 °C were chosen as initial test conditions. This temperature profile for the test specimen resulted in a water condensation rate of 0.81 mL/(m^2 s) and surface temperature ($T_{surface}$) of 42.5 °C. These initial conditions were chosen based on two main reasons. First, it represents the condition where the condensate droplet renew process was one of the fastest studied by De Carvalho et al. (2019) and Folena et al. (2020), hence producing a particularly high corrosion rate which would enable the performance of the inhibitor to be clearly evaluated. Second, previous electrochemical results using the miniature electrode configuration showed that this condition led to very stable electrochemical responses for continuous measurement, enabling the efficiency of the inhibitor to be determined as accurately as possible.

Corrosion monitoring tests were performed for 20 h in total in CO$_2$-saturated 3.5 wt% NaCl solutions. In experiments where corrosion inhibitor was applied, test specimens were pre-corroded for 4 h prior to addition of 20 ppm$_v$ of 2-ME, direct into the bulk solution

In order to ensure the 2-ME concentration measured in the condensate was not affected by oxidation of mercaptoethanol when in contact

Table 2
Chemical composition of API 5 L X65 steel.

C (wt%)	Si (wt%)	Mn (wt%)	P (wt%)	S (wt%)	Cr (wt%)	Ni (wt%)	Mo (wt%)	Al (wt%)	Cu (wt%)	Co (wt%)	Ti (wt%)	V (wt%)	Fe (wt%)
0.180	0.170	0.640	0.015	0.013	0.040	0.030	<0.002	0.017	0.013	0.018	0.002v	<0.001	Balance

with Fe^{2+} ions, from steel corrosion, acetal samples were utilized under the same conditions. The condensate samples were collected as previously described. The tests matrix is presented in Table 3.

2.5. 5,5′-dithiobis-(2-nitrobenzoic acid) (DTNB) colorimetric technique for thiol quantification

Alkylthiols are highly susceptible to oxidation in the presence of molecular oxygen, particularly at high pH. Hence, a rapid technique to competently quantify the concentration of this chemical is required.

Ellman's Reagent, 5,5′-dithiobis-(2-nitrobenzoic acid) or DTNB, is routinely used as a bio-chemical technique for quantification of thiol-containing compounds in pure solutions and biological samples. Ellman's reagent can also be used to quantify the number of thiol groups on proteins (Scientific, 2024). In this paper, the methodology associated with the use of this use of this colorogenic compound was adapted for residual analysis in TLC applications.

DTNB (Fig. 3) is a water-soluble compound that produces a measureable yellow-colored product when it reacts with thiols. The reagent specifically targets –SH groups, and possesses a high molar extinction coefficient and short reaction time (Barker, 2012).

In terms of the specific reaction, DTNB reacts with free thiol groups to produce a mixed disulfide and 2-nitro-5-thiobenzoic acid by targeting the conjugate base (R-S-) of the free thiol group. TNB is produced from the reaction (Fig. 4) which is effectively the "colored" species as it has a high molecular extinction coefficient in the visible range.

Ellman's Reagent solution was prepared by dissolving 4 mg of DTNB in 1 ml of 0.1 mol tris(hydroxymethyl)aminomethane (Tris) reaction buffer at pH 8.0.

For the residual analysis technique presented in this paper, 100 μL of collected condensate was combined with 13.7 μL of Ellman's Reagent, and left for 10 min. The level of absorbance was subsequently measured using a spectrophotometer set to 410 nm.

Before every residual analysis measurement, calibration curves were generated using known concentrations to establish the relationship between absorbance and concentration for 2-ME. A 2-fold dilution series was prepared in a 96 well plate with 2-ME in the respective tested solution (i.e., CO_2-saturated solution) over concentrations ranging from 0 to 31.25 ppm$_v$. Two independently developed calibration curves are depicted in Fig. 5, highlighting the strong linear correlation between concentration and absorbance at 410 nm.

The water condensate and bulk solution were collected at different times after addition of the 2-ME (10 min, 60 min and 1,200 min), by overfilling Eppendorf vials linked to a specially integrated condensate collector. The vials were subsequently sealed and stored under refrigerated conditions (3 °C) prior to analysis shortly afterwards.

2.6. Surface characterization

In order to understand the mechanism of 2-ME as a VCI, different surface analysis methods were implemented to complement the corrosion rate data. A Carl Zeiss EVO MA15 SEM along with energy-dispersive X-ray spectroscopy (EDX) analysis was used in order to observe the corrosion morphology and features along with surface elemental composition analysis.

To obtain further information as of the potential adsorption mechanism of 2-ME, XPS was conducted using a Thermo NEXSA with an X-ray source of Al Kα and analysis spot size of 100 μm, this technique also provides chemical information with regards to any organic corrosion product film on the surface of the sample.
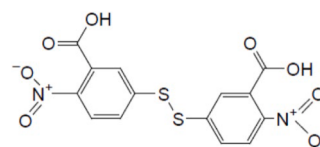

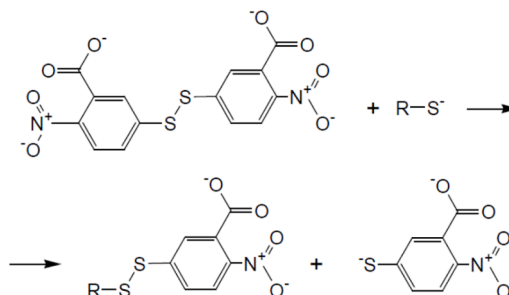**Fig. 3.** Structure of DTNB (adapted from Barker (2012)).

Fig. 4. Reduction of DTNB with a free thiol to form a mixed disulphide and TNB^{2-} (adapted from Barker (2012)).

Complementary, scanning transmission electron microscopy (STEM) coupled with EDX and Electron energy loss spectroscopy (EELS) analysis were performed using a FEI Titan Themis Cubed 300 TEM. EELS is a surface-sensitive vibrational spectroscopy which provides both compositional and chemical information being able to elucidate local chemical changes and chemical state of atoms. This characterization was used in conjunction to XPS analysis to understand the 2-ME adsorption mechanism.

3D profilometry was carried out using Bruker NPFlex 3D interferometer to analyze the roughness and extent of localized attack of the corroded surface of the mass loss specimens using a 20x magnification lens. Three mass loss specimens were analysed for each test condition
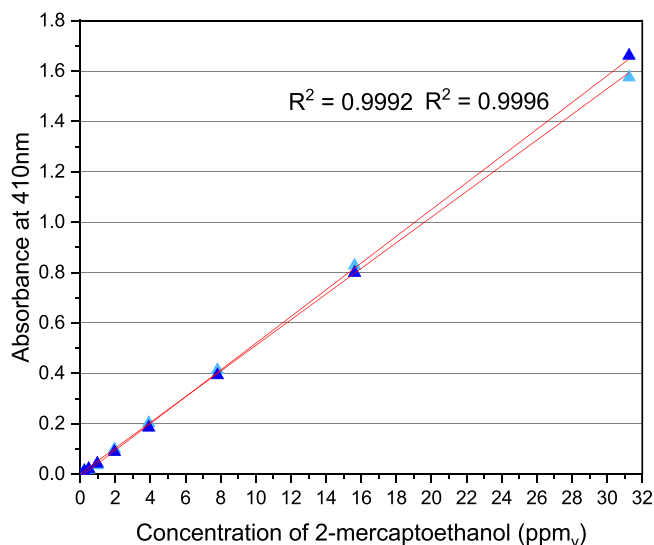

Fig. 5. Measured absorbance levels at 410 nm when 2-mercaptoethanol reacts with DTNB at concentrations between 0 and 31.25 ppm$_v$ (values of absorbance for the sample prior to the addition of the reagent have been subtracted from initial values).

Table 3
Top-of-line corrosion test matrix.

Solution composition	T_{gas}	T_{ext}	$T_{surface}$	WCR	Inhibitor concentration	Sample material
CO_2-Saturated 3.5% NaCl	80 °C	−10 °C	42.5 °C	0.81 mL/(m² s)	20 ppm$_v$ 2-ME	Acetal and X65 carbon steel

using profilometry for roughness and pitting/localized corrosion. A minimum surface area of 2×2 mm was analysed on each of the three mass loss specimens.

3. Results and discussion

3.1. Real-time, in-situ corrosion rate response in CO_2 top-of-line corrosion environment

In-situ electrochemical measurements were taken every 10 min over 20 h in a TLC environment with a WCR$=0.81$ mL/(m^2 s). These measurements facilitated real-time monitoring of the X65 carbon steel corrosion rates within the condensate both prior to, and after addition of the 2-ME. Fig. 6 shows the TLC behavior of X65 steel with 4 h-pre corrosion prior to the addition of 20 ppm$_v$ 2-ME to the bulk solution.
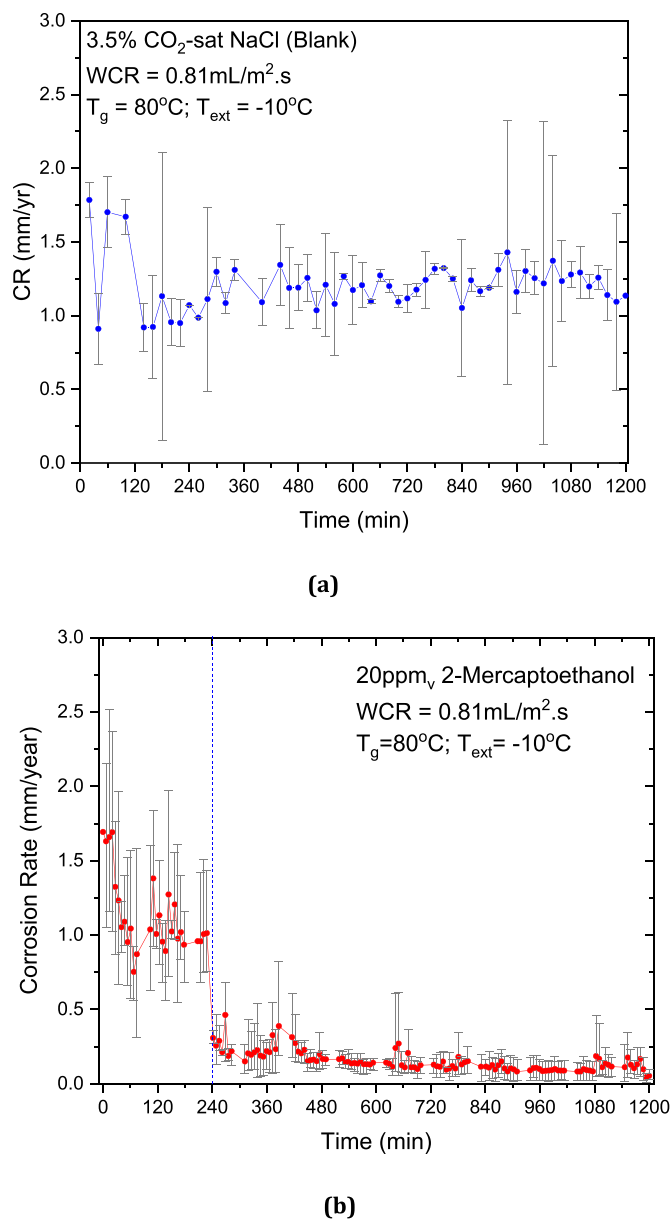

(a)

(b)

Fig. 6. Top-of-line corrosion rate over 20 h for API 5L X65 steel exposed to the vapour produced from a CO_2-saturated 3.5 wt% NaCl brine at $T_{gas} = 80$ °C, $T_{ext} = -10$ °C, $T_{surface} = 42.5$ °C and WCR = 0.81 mL/(m^2 s), (a) without addition of 2-ME (blank) and (b) with addition of 20 ppm$_v$ 2-ME at 240 min (4h-pre-corrosion). Data is achieved via the use of miniature three-electrode system positioned in the top of line condensate.

Note that the corrosion real-time corrosion rates were determined using Eqs. (1) and (2), with values of 90 and -174 mV/dec for β_a and β_c, respectively in the absence of 2-ME, and values of 61 and -80 mV/dec for β_a and β_c, respectively, in the presence of 2-ME, all based on Tafel measurements provided. Note that due to the variability of the Hastelloy reference electrode potential, the polarization responses are plotted relative to the open circuit potential of the X65 material at the measurement was performed.

The TLC corrosion rate in the tested conditions prior to adding the inhibitor averages around 1 mm/a for the first 4 h of test. This value is in agreement with results observed in open literature under similar conditions (Belarbi et al., 2017; De Carvalho et al., 2019; Islam et al., 2018) when no protective film is formed on the steel surface. As soon as 20 ppm$_v$ 2-ME is added to the bulk solution (at 240 min) the TLC rate rapidly and drastically reduces, achieving a general corrosion rate of around 0.06 mm/a after 20 h, which relates to an inhibition efficiency (IE) of 93.8%. What is important here is that the real-time electrochemical measurements provide not only the inhibited rate, but also an appreciation for the kinetics of corrosion inhibitor adsorption at the top of line system, which is also an important factor to consider in the deployment of corrosion inhibitors.

Fig. 7 provides a comparison between the dynamic polarization curves for carbon steel exposed to TLC environment at a WCR = 0.81 mL/(m^2 s) after 20 h of test with and without addition of 20 ppm$_v$ of 2-ME in the bulk solution. As stated previously, the y-axis represents the applied potential vs. the OCP at the end of each individual test.

By analysing the polarization plots it can be seen that the addition of 2-ME in the bulk solution suppressed both the anodic and cathodic reactions, in comparison to the curve obtained when no inhibitor is added into the system. These results suggest that 2-ME can be classified as a mixed type inhibitor and is in accordance with previous research (Ehteshamzadeh et al., 2006; Döner et al., 2011). These observations indicated that the adsorption of 2-ME onto the steel surface might form a barrier which mitigate the corrosion process reducing the cathodic reaction (hydrogen evolution) and anodic reaction (iron dissolution on the steel surface). Additionally, a parallel trend to lower current values after the addition of the VCI was observed, indicating that the presence of the corrosion inhibitor do no change the reactive mechanism of the cathodic reaction (Tan et al., 2023).

In order to validate the electrochemical data obtained from the miniature electrode configuration, mass loss tests were also performed
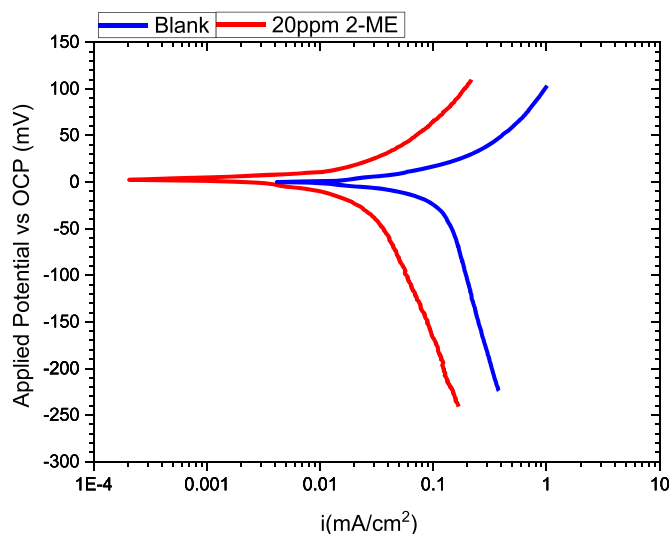

Fig. 7. Tafel polarization curves after 20 h for API 5 L X65 steel exposed to the vapour produced from a CO_2-saturated 3.5 wt% NaCl brine at $T_{gas} = 80$ °C, $T_{ext} = -10$ °C, $T_{surface} = 42.5$ °C and WCR = 0.81 mL/(m^2 s) with and without addition of 20 ppm$_v$ 2-ME at 240 min (4 h pre-corrosion).

with and without addition of 20 ppm$_v$ 2-ME after 4 h into the experiment. The average corrosion rate obtained after 20 h based on gravimetric analysis is presented in Fig. 8 and compared with the average corrosion rate values obtained via the implementation of electrochemical techniques during 20 h of test.

Both mass loss and electrochemical results are in agreement to one another. Regarding mass loss tests, the addition of 20 ppm$_v$ of 2-ME with 4 h pre-corrosion resulted in a reduction of the corrosion rate from 1.2 to 0.18 mm/a, resulting in an inhibitor efficiency of 85%, agreeing well with the efficiency of 93.8% determined from the average electrochemical corrosion rate response.

It is important to stress that the inhibitor efficiency determined in each of these cases is affected somewhat by the initial 4 h of pre-corrosion. This undoubtedly creates a higher mass loss than would be expected for experiments in the presence of 2-ME, resulting in an underestimate of true inhibitor efficiency (calculated at around 94% from real time electrochemical measurement). Indeed, subtracting an estimated mass loss for 4 h pre-corrosion at 1.2 mm/a from the mass loss data in Fig. 8, followed by recalculating the average corrosion rate over the remaining 16 h of the experiment produces a rate of 0.07 mm/a. This value aligns very well with rates predicted from the electrochemical response in Fig. 6, particularly towards the latter stages of the experiment, helping further reinforce the validity of the data acquired through electrochemical measurement.

Finally, as a means of comparison with other thiol inhibitors, previous studies using 100 ppm$_v$ and 400 ppm$_v$ longer chain alkanethiols (hexanethiol, decanethiol and mercaptoundeanoic acid) conducted by Belarbi et al. (2017) observed a reduction of the TLC rate from 1 mm/a to between 0.02 mm/a and 0.13 mm/a at a WCR = 0.6 mL/(m^2 s), T_{gas} = 65 °C and sample temperature of 32 °C. Hence, the levels of inhibition efficiency are comparable with those reported here.

3.2. Residual analysis quantification of thiol as a VCI in the condensate

Although effective inhibition of general corrosion from 2-ME is observed, the question still remains as to the exact inhibition mechanism, and the degree of protection afforded by the molecule against localized corrosion. In relation to the inhibition mechanisms, this can be divided into t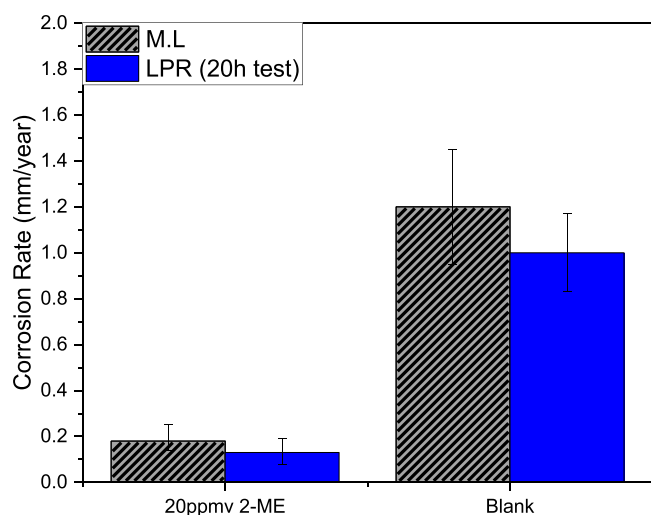wo stages: 1) the co-condensation of 2-ME within the condensate, and 2) the adsorption at the steel-electrolyte interface.

In an effort to understand the first stage, both condensate and bulk solution samples were collected at the end of each TLC test and measured using the adapted DTNB assay outlined previously. The average concentration of 2-ME that partitions to the top of the line water condensate and the control concentration of inhibitor in the bulk solution is referred in Fig. 9, along with the associated maximum and minimum error from a minimum of three measurements. As a control, additional condensate samples were taken in the absence of X65 steel coupons, with acetal specimens used in their place. This was undertaken to check/validate whether the presence of dissolved cations (Fe^{2+}) significantly influences the measurement technique.

As shown in Fig. 9, with a total of 19.14 ppm$_v$ ± 1.5 of 2-ME added to the bulk solution, a concentration of 12.7 ppm ± 0.97 is achieved in the condensate; a partition coefficient of 0.66. Additionally, the results within Fig. 9 for the system with acetal test samples suggests that the presence of Fe^{2+} did not significantly interfere in the application of the assay, since in both tests with and without the presence of Fe^{2+} ions the quantity of VCI that partitioned to the condensate were within error.

3.3. 2-ME adsorption mechanism — surface microscopy and spectroscopy characterisation

The adsorption mechanism of thiols on metal surface is a subject of differing opinion/observation depending on the thiol molecule (length, geometry, and additional groups), the thiolate position, the metal substrate and the corrosive media (Ehteshamzadeh et al., 2006; Bentis et al., 2005; Ruan et al., 2002). Most research calculate the adsorption behaviour through thermodynamic parameters. However, studies have been carried out observing the chemisorption of thiols and derivatives, mostly on coper surface through spectroscopy measurements such as XPS, atomic force microscopy (AFM) and high-angle annular dark-field (HAADF)-EDX.

In 2013 a research group studied the surface chemical structure and composition of adsorbed 2-mercaptobenzimidazole (MBIH) on cooper using angle-resolved XPS. It was found that MBIH molecules chemisorbs on the Cu surface through their N and S atoms. The MBIH layer thickness is 1.9 ± 0.5 nm, as determined from a detailed analysis of the background in the XPS spectra. Tentative MBIH orientations on Cu were suggested based on the XPS measurements (Finšgar, 2013).
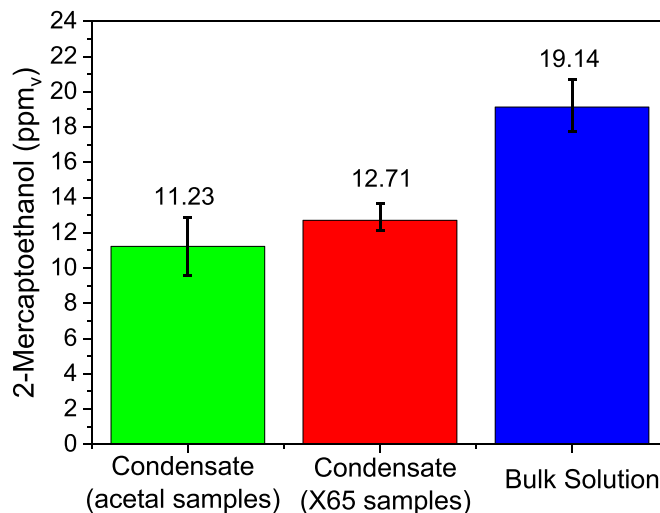

Fig. 8. Comparison between mass loss and electrochemical top-of-line corrosion rate over 20 h for API 5 L X65 steel exposed to the vapour produced from a CO_2-saturated 3.5 wt% NaCl brine at a WCR = 0.81 mL/(m^2 s) at blank and with addition of 20 ppm$_v$ 2-ME 4 h pre-corrosion. Error bars represent the maximum and minimum mass loss values and the maximum and minimum determined average corrosion rates from each experiment.

Fig. 9. 2-ME concentration determined within the condensate and bulk fluid using DTNB assay. Control tests with acetal test specimens were performed to observe the potential influence of dissolved Fe^{2+} ions on the performance/reliability of the technique.

Another study regarding 2-mercaptobenzimidazole (2-MBI) as a corrosion inhibitor for copper was conducted to understand its corrosion inhibitor properties and its SAM behaviour. Using Auger Electron Spectroscopy, Scanning Tunneling Microscopy and X-ray Photoelectron Spectroscopy, it was observed the formation and adsorption of a monolayer with S and N (from the thiol and the imidazoline, respectively) bonded to the Cu surface (Wu et al., 2020).

Anadebe et al. (2022) recently published a study on sulphur-doped polymeric nanomaterial as SAM corrosion inhibitor for X65 steel in CO_2 environment. Detailed physiochemical characterization was carried out using X-ray diffraction (XRD), Raman, Fourier transform infrared (FTIR), ultraviolet-visible (UV), and XPS. The appearance of Fe-S via the XPS analysis corroborated for the hypothesis of chemisorption of the corrosion inhibitor through the sulphur acting as a head group (Anadebe et al., 2022).

In an effort to understand the mode of interaction between 2-ME and X65 carbon steel in this study, a series of microscopic and spectroscopic analytical techniques were implemented.

SEM coupled with EDX analysis, was performed on samples subject to 20 h tests to initially observe the surface morphology due to addition of 20 ppm_v 2-ME. Two different types of signals, secondary electron (SE) and backscattered-electron (BSE) were used in the acquisition of the SEM images in order to better characterize both the topography morphology and distinguish between different phases (Fig. 10). From
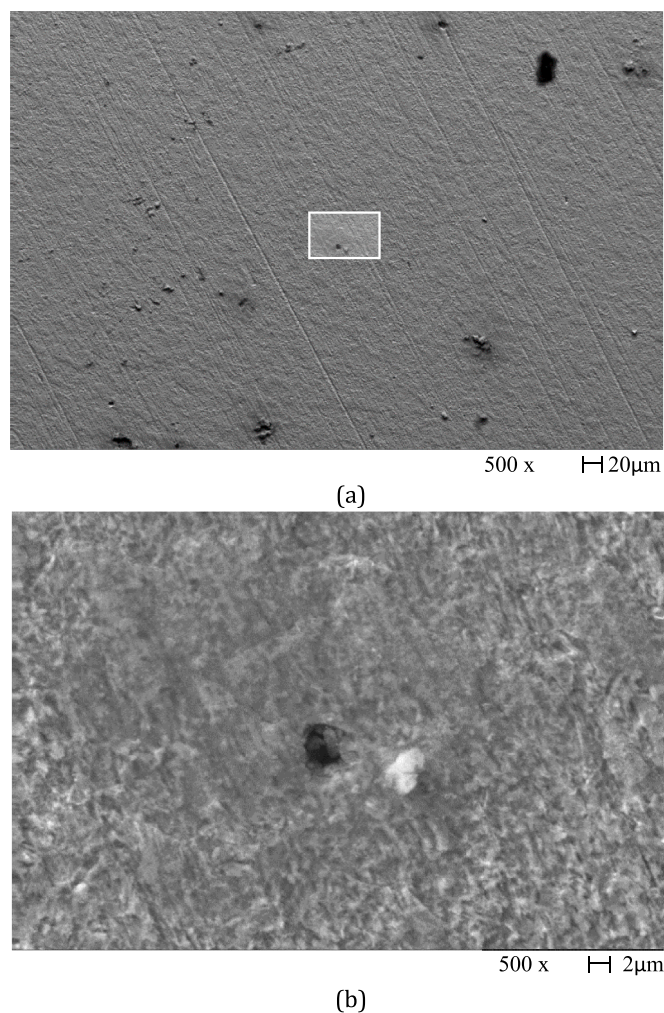

500 x   ⊢⊣20μm

(a)

500 x   ⊢⊣2μm

(b)

Fig. 10. SEM analysis after 20 h tests with 4 h pre-corrosion and addition of 20 ppm_v 2-ME: (a) back scattered-electron (BSE) image at 500x magnification, and (b) pit-like feature detail secondary electron (SE) image at 5,000x magnification.

these images, it is possible to still observe the grinding marks resulting from initial sample preparation, corroborating with the high inhibition efficiency of 2-ME.

Reviewing Fig. 10 more closely, a series of round, darker features surrounded by a darker film were observed sparsely on the steel surface. Careful analysis using both SE and BSE beams was performed in order to understand if such features are indication of pits. The magnified image in Fig. 10 combined with EDX analysis (Fig. 11) suggests these are corrosion product/surface deposits which are rich in oxygen. Further analysis of pitting and localized corrosion is presented in a subsequent section.

The EDX analysis shown in Fig. 11 reveals that the X65 steel exhibits a clear reading of sulphur across the entire surface as a result of 2-ME adsorption. As previously mentioned, it is possible to observe regions rich in oxygen (and possibly sulfur) which might be a result of local formation of corrosion products/deposits.

In reference to the observations here, when studying iron surfaces modified by *n*-decanethiol and *n*-propanethiol, Volmer and Stratman observed that during the transfer from the test cell to surface analysis (XPS and Auger chambers) oxygen adsorbed on and oxidized part of the iron surfaces which were free of chemisorbed thiol molecules. Such contamination and adsorption of oxygen thin layer had the form of small islands between chemisorbed organic molecules.

To further understand the 2-ME inhibitor film and mode of adsorption on the steel surface, XPS analysis was performed. Fig. 12 presents the S 2p and Fe 2p spectra and their respective deconvoluted peaks. From literature it is stated that metallic surfaces adsorbed with thiols should show S 2p signals at binding energies between 160 eV and 170 eV (Volmer-Uebing and Stratmann, 1992.) For Fe 2p fitting, a more careful evaluation must be made since transition metals have complicated electronic structures with multiple valences and investigations regarding thiols adsorption on iron/steel substrate is not particularly common.

Regarding Fig. 12(a), a multiplets splitting is observed with two high intensity peaks at binding energies (BEs) of 161.97 eV, and 163.37 and 164.8 eV. These values are consistent to the binding energies of S 2p for small-chain-thiol monolayers adsorbed on iron (sulphur-iron bond) and free mercaptans groups, respectively (Volmer-Uebing and Stratmann, 1992; Ruan et al., 2002).

The high intensity of SH which accounts for high quantities of thiol on the surface might be an indication of a fully saturated sulfur layer on the surface of the analyzed samples. This would be consistent with the Langmuir isotherm method for monolayers in which adsorption uniformly occurs until the entire surface area is coated with a single layer of molecules and no further adsorption can occur (Langmuir, 1918; Tiab and Donaldson, 2016). However, to assure such statement further tests regarding isotherm fitting should be performed.

The presence of sulfonates and sulfinates at higher BE (i.e. 166.42 eV and 168.00 eV) are probably due to oxidation of the surface when exposed to the lab air before performing XPS analysis. This observation was also done by Vericat et al. (2008) when characterizing SAMs from butanethiol capped gold surfaces. Same oxidation degradation was observed on Ag, Cu, Ge, and Pt surfaces when characterizing different thiols SAMs (i.e. 1-Alkanethiols, metanethiol, 1-octadecanethiolate) (Vericat et al., 2014; Ardalan et al., 2010; Telegdi, 2020; Sashuk, 2012).

Two different studies analysed the adsorption mode of thiols self-assembled monolayers on iron Volmer-Uebing and Stratmann, 1992 and 316 L stainless steel Ruan, C.M., Bayer, T., Meth, S., Sukenik, C.N., 2002) both studies observed a high intensity peak at 161.8 ± 0.2 eV on S 2p XP spectra, interpreted as a direct Fe-S bond. The authors considered it as a sulphur-anchored film (chemisorption) through cleavage of the S-H hydrogen.

Fig. 12(b) represents the qualitative peak-fitting analysis for Fe 2p XP spectrum regarding both Fe $2p_{3/2}$ and $_{1/2}$. Binding energies fitting were performed upon careful consultation of both published literature, and National Institute of Standards and Technology (NIST) standard database (NIST, 2000).
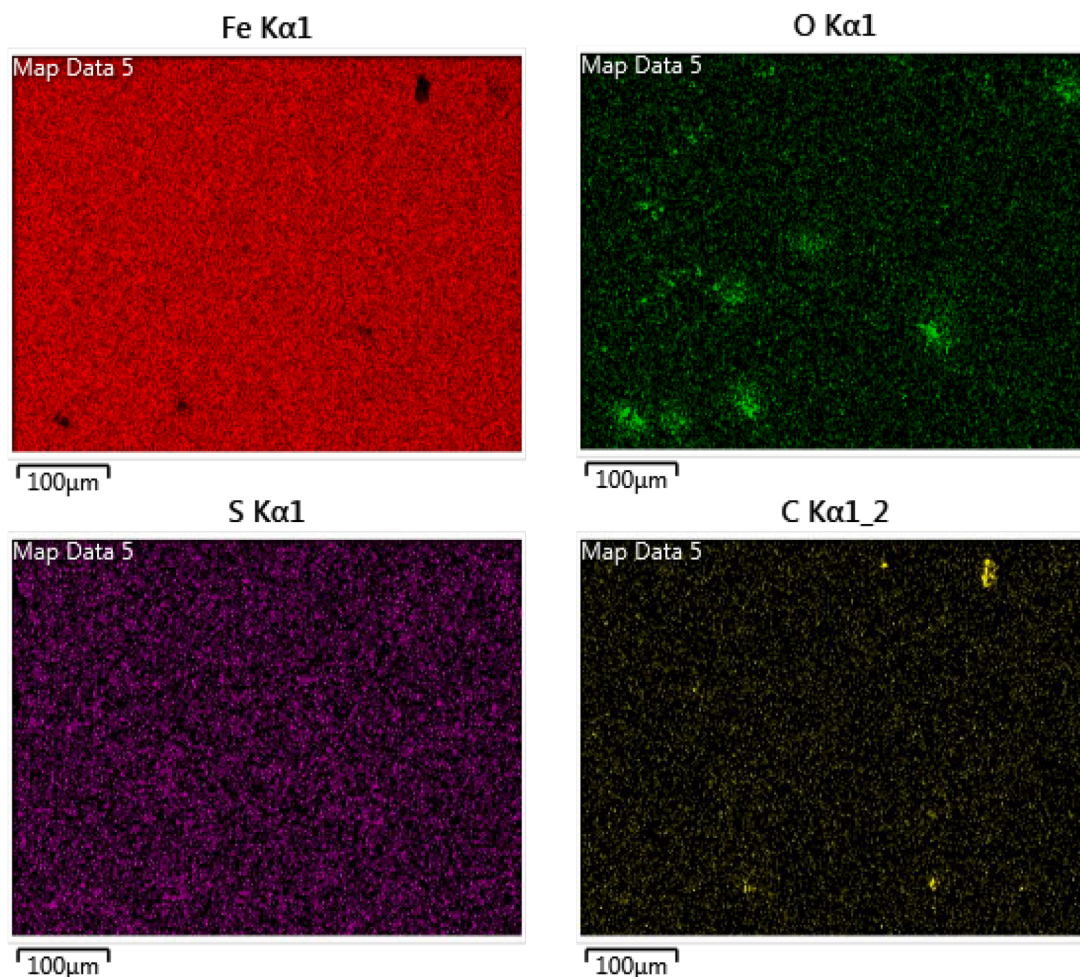
Fig. 11. EDX compositional analysis of X65 carbon steel samples tested in CO_2 saturated TLC environment with presence of 20 ppm_v 2-ME.
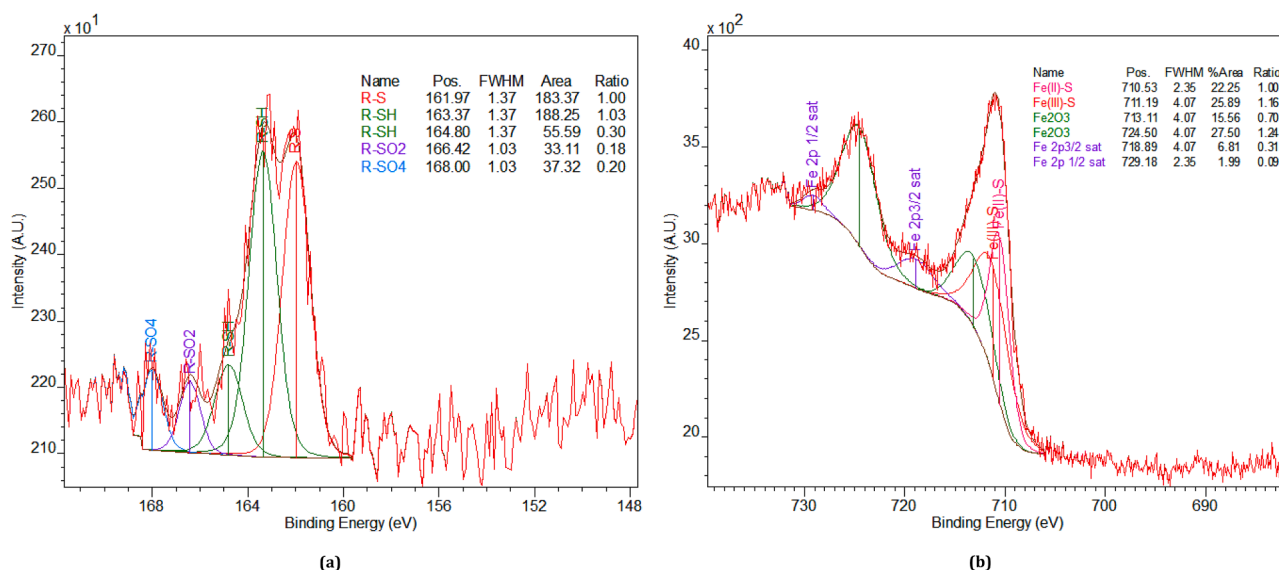

Fig. 12. XP spectra of the surface of API X65 steel samples after TLC test with addition of 20 ppm_v 2-ME after 4 h pre-corrosion, (a) S 2p spectrum, and (b) Fe 2p spectrum.

In order to ensure a reasonable and scientifically viable fit both Fe $2p_{3/2}$ and Fe $2p_{1/2}$ regions were deconvoluted with the minimum number of synthetic peaks possible (Matamoros-Veloza et al., 2018). At Fe $2p_{3/2}$ region, a triplet was used to fit the high intensity peak for

monosulfides and Fe (III) oxide at BEs 710.53 eV, 711.19 eV, and 713.11 eV, respectively, and a single broad peak at 718.89 eV which is a satellite peak for this region. For the higher BE region (Fe $2p_{1/2}$), a single was fitted for the main peak for Fe^{3+} oxide species, 724.50 eV, and a broad
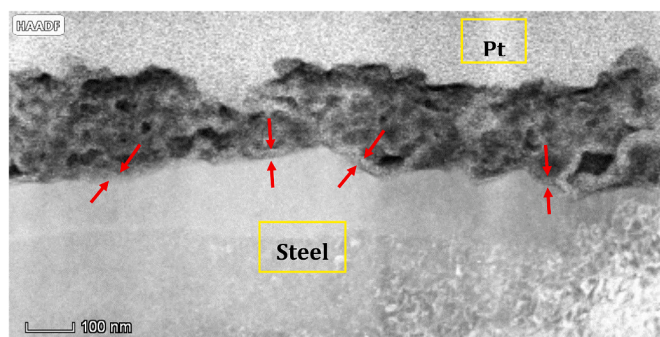
Fig. 13. HAADF-STEM cross-section image of API X65 steel exposed to CO_2 TLC environment at WCR = 0.81 mL/(m^2 s) with 4 h pre-corrosion and addition of 20 ppm$_v$ 2-ME for 20 h. Red arrows indicate compact thin sulphur-rich layer underneath a porous amorphous layer.

peak was observed at 729.18 eV and was related to Fe 2p$_{1/2}$ satellite according to Corrales-Luna et al. (2017). The sulfide double synthetic peaks are in accordance to binding energies fitted by Carver et al. (1972) when studying bonding energies for Cr, Mn, Co and Fe, for Fe^{II}-S; and by Matamoros-Veloza et al. (2018) for FeS nano particles, for Fe^{III}-S. The presence of Fe-S binding was also observed in the S 2p spectra and once again corroborates for the assumption of chemisorption of thiol on the carbon steel sample.

Furthermore, attention must be brought for the oxide species fitting. Fe_2O_3 and $FeSO_4$ have binding energies within proximity (724.4 eV and 724.3 eV, respectively). Hence, since SO_4^{2-} ions were observed at S 2p, it could be the case for Fe 2p analysis that both oxides energies are overlapping due to the complexity of the system.

As expected, for first row transitional metals as Fe, especially in mixed metal and metal oxide systems, a multiplet splitting and satellite peak was observed due to presence of unpaired electrons (Biesinger et al., 2011). However, by a combined analysis of both Fe 2p and S 2p, it is possible to observe that at both regions the presence of Fe-S bonds as well as the formation of oxide layers due to lab air contamination, as

seen in EDX images.

As a final form of surface characterization, TEM and EDX analysis of the sample cross-section exposed to 20 h of TLC with addition of 20 ppm$_v$ 2-ME was performed and is presented in Figs. 13 and 14.

From Fig. 13 it is possible to observe an amorphous film adsorbed on the steel substrate with a total thickness of 200 nm, composed of two layers; an inner more compact and ultra-thin layer, close to the substrate, and a thicker porous layer on top of the previous one.

As observed in the elemental map acquired through EDX-STEM (Fig. 14), the corrosion film is mainly formed by sulphur, carbon and iron. The presence of sulphur is due to the 2-ME thiol inhibitor, whilst the great amount of carbon on the corrosion film can be either attributed to the presence of iron carbide (already residing within the steel microstructure), excess of hydrocarbonate on the sample surface (thiol) and/or contamination during focused ion beam (FIB) sectioning. The EDX map relating to sulphur in Fig. 14 highlights the presence of ultrathin layer sitting close to the steel interface.

3.4. Corrosion inhibition response of 2-ME for localized top-of-line corrosion

A crucial requirement of TLC inhibitors is to mitigate localised corrosion, as partial and/or poorly efficient inhibitors are capable of exacerbating corrosion. As such, 3D interferometry was used to analyse the surfaces of X65 subjected to TLC conditions in the presence of 2-ME. In order to assess pit growth susceptibility more rigorously, tests were performed at both 20 h and 96 h. An example of one test for each test duration is presented in Fig. 15.

Regarding the 20 h tests no pits were observed on the tested samples. All the samples presented a smooth surface profile with an average roughness of 0.2 μm. Although some scarcely localized features were found, as shown on the profilometry of Fig. 15(a), with the deepest feature of only 5 μm. When analysing such features in relation to pit parameters (i.e. diameter and depth) for active materials and considering ASTM G46–21 (2021) standard there weren't enough deep pits to calculate the standard average for pit damage. Hence, such features might be due to the preferential ferrite consumption during the 4 h pre-corrosion prior to addition of inhibitor.
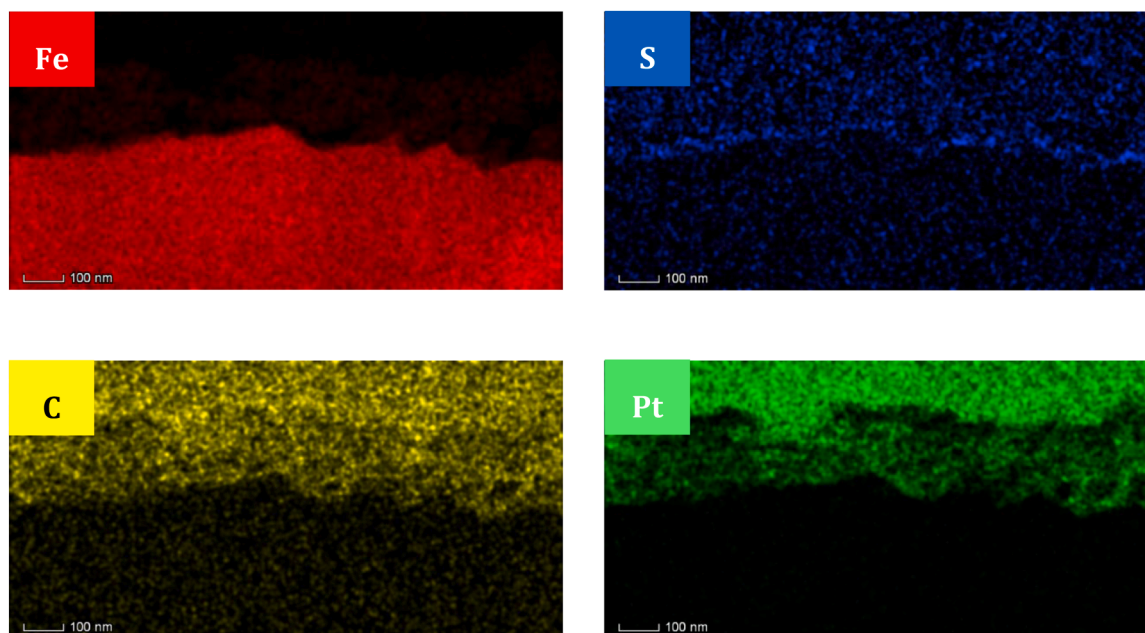

Fig. 14. EDX mapping of HAADF-STEM sample showing the elemental composition of corrosion product. Platinum (Pt) layer was added during FIB section to protect the corrosion film.
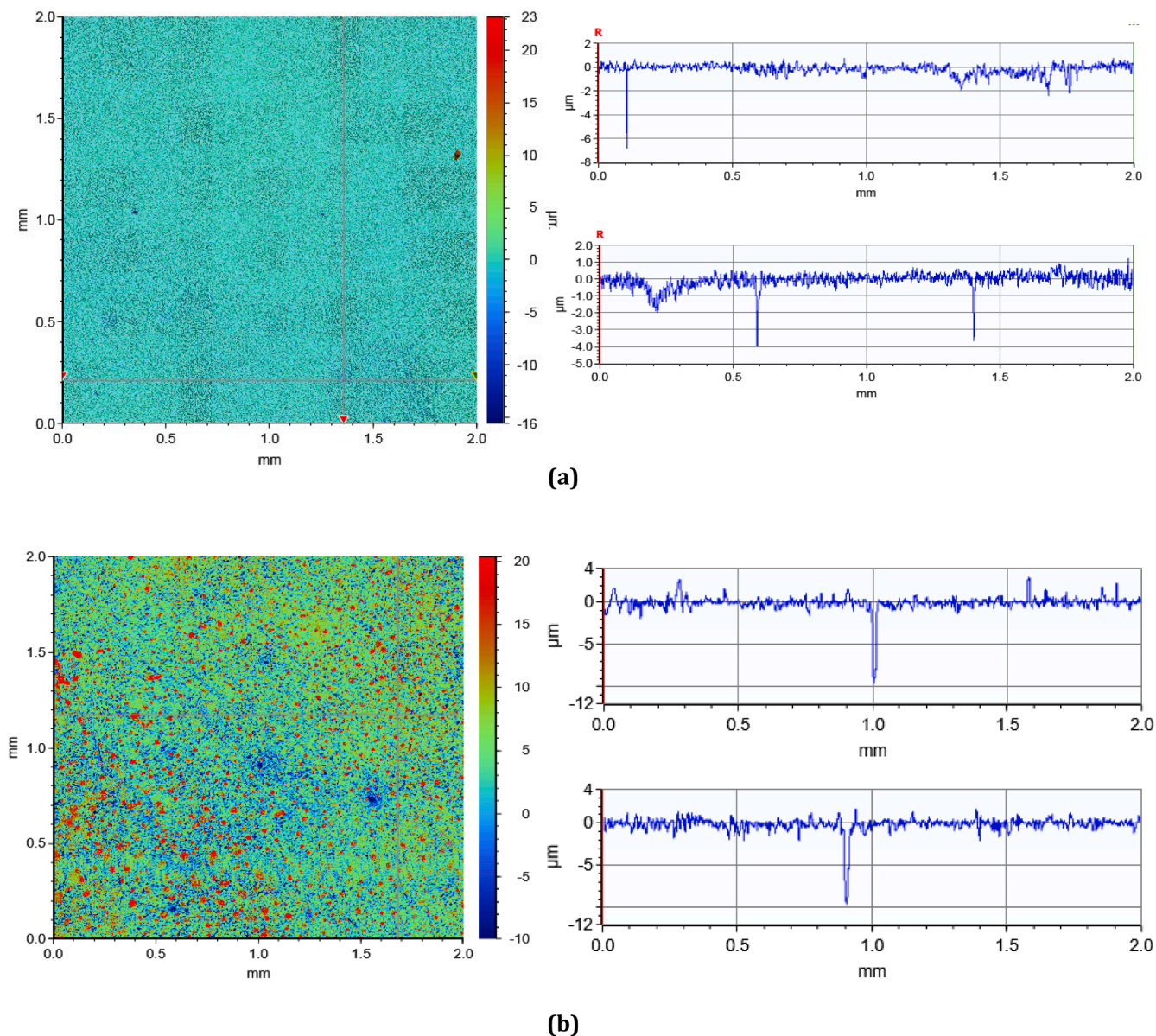
(a)

(b)

Fig. 15. 3D profilometry analysis of API X65 steel exposed to CO_2 TLC environment at WCR = 0.81 mL/(m^2 s) with 4 h pre-corrosion and addition of 20 ppm_v 2-ME at (a) 20 h test and (b) 96 h test.

Long term tests showed a rougher surface with an average roughness of 0.3 μm. Additionally, the dense black film observed on the top of the sample surface, was strongly attached and difficult to remove.

On the analysed surface area of 2×2 μm, only one isolated random allocated pit with an average depth 10.0 μm was observed in some of the samples. Scarcely localized features were also observed for the long term tests samples, with average depth of 2.6 μm. However, such depth is not considered as pit depths for active materials as carbon steel, since general corrosion is also taking place and these depths could be related to preferential ferrite corrosion (Pessu et al., 2015).

From these results, it is possible to confirm that the addition of 20 ppm_v 2-mercaptoethanol on the bulk solution at CO_2 top of line corrosion systems is efficient for protection of both general and localized corrosion under the conditions considered. These results are in agreement with those of Belarbi et al. (2018) who observed the protective ability of longer chain thiols against localized corrosion with an addition of 400 ppm_v of inhibitor.

4. Conclusions

This study evaluated the behaviour of 2-ME as a potential volatile corrosion inhibitor against CO_2 top-of-line corrosion (general and pitting corrosion) of an API X65 carbon steel. Experimental results were collected through a combination of real time electrochemical measurements, biochemical techniques, and surface characterization to assess the co-condensate behaviour and inhibition efficiency of 2-ME. Results showed that 2-ME effectively acts as corrosion inhibitor in CO_2-TLC environment by chemically adsorbing on sample surface and mitigating the corrosion process with an inhibitor efficiency of 94% in the conditions studied.

1) The addition of 20ppm_v of 2-ME to the TLC system resulted in the corrosion rate decreasing from about 1.2 mm/a to 0.06 mm/a resulting in a corrosion IE of 93.8% even after 4 h of pre-corrosion of the samples.

2) 2-ME acts as a mixed-type corrosion inhibitor with suppression of both anodic (iron dissolution) and cathodic (hydrogen evolution) reaction(s).

3) The proposed biochemical assay showed to be a reliable and rapid technique for quantification of thiol-based VCI in top-of-line corrosion environments, enabling inhibitor doses optimization.

4) From a total of 20 ppm of 2-ME added in the bulk solution only 66% (about 12 ppm) of the chemical reaches the top of line region and effectively takes part in the formation of a self-assembled monolayer to protect the steel from corrosion.

5) SEM images showed minor corrosion attack features due to the corrosion inhibitor efficiency. EDX images showed the presence of sulphur related to the absorbed thiol.

6) STEM coupled with EDX showed a multilayer like at the sample cross-section. A ultra-thin, more compact inner layer was found being related to the 2-ME.

7) XPS analysis showed the presence of peaks at BEs related to small-chain-thiol monolayers adsorbed on iron (Fe-S bond) and free mercaptans groups (-SH), which might indicate a chemical adsorption of 2-ME film on the steel surface.

8) No localised corrosion was observed after both 20 h and 96 h tests. The scarcely observed localized deep features do not allow qualification as pitting corrosion according to ASTM G-46 (2021).

CRediT authorship contribution statement

Mariana C. Folena: Writing – review & editing, Writing – original draft, Methodology, Investigation, Formal analysis, Data curation, Conceptualization. **Joshua Owen:** Writing – review & editing. **Iain W. Manfield:** Writing – review & editing, Data curation. **Hanan Farhat:** Writing – review & editing, Funding acquisition. **J.A.C. Ponciano:** Writing – review & editing, Supervision, Resources, Project administration, Funding acquisition, Conceptualization. **Richard Barker:** Writing – review & editing, Supervision, Resources, Project administration, Funding acquisition, Conceptualization.

Declaration of competing interest

The authors declare that they have no known competing financial interests or personal relationships that could have appeared to influence the work reported in this paper.

Acknowledgement

References

Anadebe, V.C., Chukwuike, V.I., Selvaraj, V., Pandikumar, A., Barik, R.C., 2022. Sulfur-doped graphitic carbon nitride (Sg-C3N4) as an efficient corrosion inhibitor for X65 pipeline steel in CO2-saturated 3.5% NaCl solution: electrochemical, XPS and Nanoindentation Studies. Process Saf. Environ. Protec 164, 715–728.

Ardalan, P., Sun, Y., Pianetta, P., Musgrave, C.B., Bent, S.F., 2010. Reaction mechanism, bonding, and thermal stability of 1-alkanethiols self-assembled on halogenated Ge surfaces. Langmuir 26 (11), 8419–8429.

ASTM, G., 2004. Standard Practice For Calculation of Corrosion Rates and Related Information from Electrochemical Measurements. ASTM International, West Conshohocken, USA, pp. G102–G189.

ASTM G46-21, 2021. Standard Guide for Examination and Evaluation of Pitting Corrosion. https://www.astm.org/g0046-21.html.

Barker, R.J., 2012. Erosion-corrosion of Carbon Steel Pipework On an Offshore Oil and Gas Facility. University of Leeds.

Behpour, M., Mohammadi, N., 2012. Investigation of inhibition properties of aromatic thiol self-assembled monolayer for corrosion protection. Corros. Sci 65, 331–339.

Belarbi, Z., George, B., Moradighadi, N., Young, D., Nesic, S., Singer, M., Nogueira, R.P., 2018. Volatile corrosion inhibitor for prevention of black powder in sales gas pipelines. CORROSION, Phoenix, Arizona, USA.

Belarbi, Z., Singer, M., Young, D., Farelas, F., Vu, T., Nesic, S., 2017. Thiols as volatile corrosion inhibitors for top of the line corrosion. NACE CORROSION. NACE.

Bentis, C.A., Zotos, A., Petridis, D., 2005. Production of fish-protein products (surimi) from small pelagic fish (Sardinops pilchardusts), underutilized by the industry. J. Food Eng 68 (3), 303–308.

Biesinger, M.C., Payne, B.P., Grosvenor, A.P., Lau, L.W., Gerson, A.R., Smart, R.S.C., 2011. Resolving surface chemical states in XPS analysis of first row transition metals, oxides and hydroxides: cr, Mn, Fe, Co and Ni. Appl. Surf. Sci 257 (7), 2717–2730.

Carver, J., Schweitzer, G., Carlson, T.A., 1972. Use of X-ray photoelectron spectroscopy to study bonding in Cr, Mn, Fe, and Co compounds. J. Chem. Phys. 57 (2), 973–982.

Corrales-Luna, M., Olivares-Xometl, O., Likhanova, N.V., Ramírez, R.E.H., Lijanova, I.V., Arellanes-Lozada, P., et al., 2017. Influence of the immersion time and temperature on the corrosion of API X52 steel in an aqueous salt medium. Int. J. Electrochem. Sci 12 (7), 6729–6741.

De Carvalho, S., Barker, R., Folena, M., Al-Khateeb, M., Mohammed, K., Gomes, J., et al., 2021. An experimental investigation of top-of-line corrosion in a static CO₂ environment. Corrosion 77 (5), 515–525.

De Carvalho, S., Hua, Y., Barker, R., Huggan, M., Gomes, J.G., Neville, A., 2019. Development and evaluation of miniature electrodes for electrochemical measurements in a CO₂ top of line corrosion environment. Corros. Eng., Sci. Technol 54 (7), 547–555.

Döner, A., Solmaz, R., Özcan, M., Kardaş, G., 2011. Experimental and theoretical studies of thiazoles as corrosion inhibitors for mild steel in sulphuric acid solution. Corros. Sci 53 (9), 2902–2913.

Ehteshamzadeh, M., Shahrabi, T., Hosseini, M., 2006. Synergistic effect of 1-dodecane-thiol upon inhibition of Schiff bases on carbon steel corrosion in sulphuric acid media. Anti-Corros. Methods Mater 53 (3), 147–152.

Feng, X., Fryxell, G.E., Wang, L.Q., Kim, A.Y., Liu, J., Kemner, K.M., 1997. Functionalized monolayers on ordered mesoporous supports. Science 276 (5314), 923–926.

Finšgar, M., 2013. 2-Mercaptobenzimidazole as a copper corrosion inhibitor: part II. Surface analysis using X-ray photoelectron spectroscopy. Corros. Sci 72, 90–98.

Folena, M.C., Barker, R., Pessu, F., Ponciano, J.A.D.C., Nevilleo, A., 2020. CO₂ top-of-line-corrosion; assessing the role of acetic acid on general and pitting corrosion. Corrosion 77 (3), 298–312.

Islam, M.M., Pojtanabuntoeng, T., Gubner, R., 2018. Study of the top-of-the-line corrosion using a novel electrochemical probe. Corrosion 74 (5), 588–598.

Kudelski, A., 2003. Chemisorption of 2-mercaptoethanol on silver, copper, and gold: direct Raman evidence of acid-induced changes in adsorption/desorption equilibria. Langmuir 19 (9), 3805–3813.

Langmuir, I., 1918. The adsorption of gases on plane surfaces of glass, mica and platinum. J. Am. Chem. Soc. 40 (9), 1361–1403.

Matamoros-Veloza, A., Cespedes, O., Johnson, B.R., Stawski, T.M., Terranova, U., de Leeuw, N.H., et al., 2018. A highly reactive precursor in the iron sulfide system. Nat. Commun 9 (1), 3125.

Musa, A.Y., Kadhum, A.A.H., Mohamad, A.B., Takriff, M.S., Daud, A.R., Kamarudin, S.K., 2010. On the inhibition of mild steel corrosion by 4-amino-5-phenyl-4H-1, 2, 4-trizole-3-thiol. Corros. Sci 52 (2), 526–533.

NIST, 2000. In: NIST X-ray Photoelectron Spectroscopy Database, NIST Standard Reference Database Number 20, Gaithersburg MD, p. 20899. https://dx.doi.org/10.18434/T4T88K.

Pessu, F., Barker, R., Neville, A., 2015. The influence of pH on localized corrosion behavior of X65 carbon steel in CO₂-saturated brines. Corrosion 71 (12), 1452–1466.

Quan, Z., Chen, S., Li, Y., Cui, X., 2002. Adsorption behaviour of Schiff base and corrosion protection of resulting films to copper substrate. Corros. Sci 44 (4), 703–715.

Ruan, C.M., Bayer, T., Meth, S., Sukenik, C.N., 2002. Creation and characterization of n-alkylthiol and n-alkylamine self-assembled monolayers on 316L stainless steel. Thin. Solid. Films 419 (1–2), 95–104.

Sashuk, V., 2012. Thiolate-protected nanoparticles via organic xanthates: mechanism and implications. ACS. Nano 6 (12), 10855–10861.

Scientific, T., 2024. User Guide: Ellman's Reagent. Available from. https://www.thermofisher.com/document-connect/document-connect.html?url=https://assets.thermofisher.com/TFS-Assets%2FLSG%2Fmanuals%2FMAN0011216_Ellmans_Reag_UG.pdf.

Tan, B., Fu, A.Q., Guo, L., Ran, Y., Xiong, J.L., Marzouki, R., et al., 2023. Insight into anti-corrosion mechanism of Dalbergia odorifera leaves extract as a biodegradable inhibitor for X70 steel in sulfuric acid medium. Ind. Crops. Prod 194, 116106.

Telegdi, J., 2020. Formation of self-assembled anticorrosion films on different metals. Materials 13 (22), 5089.

Tiab, D., Donaldson, E., 2016. Shale-gas Reservoirs. Gulf Professional Publishing Houston, TX, pp. 719–774.

Uehara, J., Aramaki, K., 1991. A surface-enhanced raman spectroscopy study on adsorption of some sulfur-containing corrosion inhibitors on iron in hydrochloric acid solutions. J. Electrochem. Soc 138 (11), 3245.

Vericat, C., Benitez, G., Grumelli, D., Vela, M., Salvarezza, R., 2008. Thiol-capped gold: from planar to irregular surfaces. J. Phys. 20 (18), 184004.

Vericat, C., Vela, M.E., Corthey, G., Pensa, E., Cortés, E., Fonticelli, M.H., et al., 2014. Self-assembled monolayers of thiolates on metals: a review article on sulfur-metal chemistry and surface structures. RSC. Adv 4 (53), 27730–27754.

Volmer-Uebing, M., Stratmann, M., 1992. A surface analytical and an electrochemical study of iron surfaces modified by thiols. Appl. Surf. Sci 55 (1), 19–35.

Wu, X., Wiame, F., Maurice, V., Marcus, P., 2020. 2-Mercaptobenzimidazole films formed at ultra-low pressure on copper: adsorption, thermal stability and corrosion inhibition performance. Appl. Surf. Sci 527, 146814.

Young Soo Ahn, V.J., 2003. Mercaptoalcohol Corrosion Inhibitors. B.H.H. LLC. EditorUSA.